58930-00-105
58916-00-105

ANL/MSD/CP--91226 CONF-961040--14

Refracted X-ray Fluorescence (RXF) Applied to the Study of Thermally Grown Oxide Scales

I. Koshelev, A.P. Paulikas, B.W. Veal

Materials Science Division

Argonne National Laboratory, Argonne, IL 60439

Proceedings of the 190th Meeting of the Electrochemical Society, San Antonio, TX, October 6-11, 1996

Work supported by the U.S. Department of Energy, Basic Energy Sciences-Materials Science under Contract #W-31-109-ENG-38.

DISCLAIMER

REFRACTED X-RAY FLUORESCENCE (RXF) APPLIED TO THE STUDY OF THERMALLY GROWN OXIDE SCALES

I. Koshelev, A. P. Paulikas and B. W. Veal
Argonne National Laboratory, Argonne IL 60439, USA

Refracted x-ray fluorescence (RXF) is a relatively new technique developed for studying properties of thin films. Here, the technique is applied to the study of thermally grown oxide scales. The evolution of chromia scales on Fe-25Cr-20Ni-0.3Y alloys and the evolution of alumina scales on β-NiAl are investigated. The technique provides scale composition and depth profile information, scale thicknesses and growth rates, and information about transient phase evolution.

INTRODUCTION

Many X-ray techniques have been introduced to investigate surface and interface properties, including grazing incidence reflectivity, absorption spectroscopy, diffraction, grazing incidence fluorescence spectroscopy, and photoelectron spectroscopy (1-7). In the present work, we consider a relatively new technique, refracted X-ray fluorescence (RXF) spectroscopy (8-14). The RXF technique measures x-ray fluorescent radiation emitted from a sample at small escape angles; i.e., at angles near the critical angle for total external reflection. The technique is element specific since fluorescent radiation from each emitting species in the sample can be monitored. Surface sensitivity is highly dependent on emission angle; near-grazing angle emission probes a minimum layer thickness of about 20 Å. The maximum probe depth depends on the sample composition and energy of the emitted x-rays. For heavier 3d transition elements (e.g., Cr through Ni), penetration depths normal to the surface for K-shell X-rays fall in the range of tens of microns. These characteristics, element and depth sensitivity, make RXF a promising technique for studying thin film phenomena.

In this paper, we investigate the utility of the RXF technique for studying thermally grown chromium and aluminum oxide scales. The RXF system described in this work provides a nondestructive depth profile for most of the elements heavier than sodium which are present in the scale, allows in situ measurement of the evolution of oxide strata, allows measurement of the thicknesses of those strata and permits inferences to be drawn about rates and mechanism of oxidation. We investigate the evolution of oxide scales on the stainless steel alloy Fe-25Cr-20Ni-0.3Y (wt. %) and oxide scales on β-NiAl. These samples were heat treated in oxygen at temperatures up to 700° C to develop the scales.

EXPERIMENTAL

Instrumentation used for the RXF experiments is shown schematically in Fig. 1 (13).

Polychromatic x-radiation from a Cr target operated at 25 keV was used to illuminate the sample. The angle of incidence for the primary x-radiation was fixed at approximately 10 degrees; the illuminated area of the sample was approximately 4 mm x 8 mm. Fluorescent radiation from the sample was detected by a Si(Li) detector with energy resolution of 140 eV. The detector position could be varied from zero to five degrees relative to the plane of the sample surface. The detector aperture, defined by slits, is 2 milliradians (mr). The sample is located in a vacuum chamber with a base vacuum of 7×10^{-7} Torr. Samples were glued to a stainless steel heater block with silver paint and were cured at 70 °C for several hours.

Oxidation studies were carried out on a bulk sample of composition 55Fe-25Cr-20Ni-0.3Y (weight percent) cut from a 1 mm thick rolled sheet. The sample was ground flat and polished (finished with 0.1 micron abrasive). Oxidation studies were also made on a polished (≈10 Å rms roughness) single crystal specimen of the intermetallic compound β-NiAl oriented to expose a (110) face.

For the Fe-Cr-Ni-Y sample, fluorescence spectra were recorded at the oxidation temperature. After the sample was isothermally oxidized (for 1 to 3.5 hours), in 0.1 Torr oxygen pressure, the chamber pressure was reduced to the base vacuum. Spectra were then recorded without adjusting sample temperature. Sample temperature was increased in 100° C increments and the measurement process was repeated. The sample was not cycled to room temperature until the series of oxidation runs was completed.

The β-NiAl sample was oxidized for 5 hrs. at 600° C in 0.1 Torr oxygen and the sample was then cooled to room temperature where measurements were made. The sample temperature was monitored with a chromel-alumel thermocouple and was controlled, with 2 °C precision, at the desired oxidation temperature.

REFRACTED X-RAY FLUORESCENCE - ANALYSIS

In the RXF technique, an outgoing fluorescent electromagnetic wave is detected on the vacuum side of the solid-vacuum interface leaving that interface at small angles (from zero to several degrees). The most important quantity in the process is the index of refraction n. For X-rays, the indices of refraction for most media are slightly smaller than the index of refraction for air. The refractive index is dependent on the energy of the X-rays, electron density and absorption of the medium (15);

$$n = 1 - \delta + i\beta \qquad [1]$$

The value of the critical angle is

$$\theta_c = \sqrt{2\delta} \qquad [2]$$

In the X-ray region, δ is typically 10^{-4} to 10^{-7} and β around 10^{-6}. Consequently, critical angles usually vary from several to tens of milliradians, values experimentally easy to measure. The existence of a critical emission angle does not mean that there is no radiation into angles which are less then critical. Like the behavior of visible wavelength photons at angles near critical, the behavior of x-rays impinging near θ_c is not trivial. With a wave propagating at an angle less than critical in the medium with the larger index of refraction, there is associated an evanescent wave which propagates along the interface and is exponentially damped into the medium with the smaller index of refraction. The magnitude of the damping exponent is a function of the direction of propagation (θ in our experiment) of the wave on the other (larger n) side of the interface.

For this study, we first consider a point source of radiation inside a semi-infinite medium, with an ideally flat and smooth interface with the vacuum The fluorescence intensity, detected at angle θ with respect to the surface, which was emitted from an element present in concentration C(z) at a distance (depth) z from the surface is

$$I(\theta) = Const * \int_{\Delta} \int_{z} C(z) * I(z,\theta) * \exp(-\mu_i * z / \sin 10^\circ) dz d\theta \qquad [3]$$

Const includes factors such as the illuminating intensity, the probability of ionization of an atom of the emitting element by the illuminating radiation, the probability for emission from this excited atom, and the response of the detector. $I(z,\theta)$ is the probability (zero to one) that fluorescence radiation which originates at distance z below the surface of the specimen will reach a detector positioned at angle to the surface θ; it deals with absorption and with any reflection which might occur at the surface and at any other interface which is encountered. μ_i is the linear absorption coefficient for the illuminating x-ray radiation, 10° is the angle at which the illuminating radiation enters the sample, and Δ is the angle of acceptance (aperture) of the detector, about 2 milliradians. If layering is present, care must be taken that contributions from all layers and the substrate are properly considered. The nature of [3] has been considered by other workers employing RXF (8,16); our approach will be presented in detail in a future publication (17).

It is clear that, for small emission angles (near grazing), the fluorescence signal comes from a shallow region near the sample surface. If all elements were uniformly distributed in the bulk, the signal $I(\theta)$ would be proportional to the concentration of the element and its linear absorption coefficient. In the present work we consider all the interfaces to be ideally smooth. However, for rough interfaces the above formulas must be corrected. Several approaches have been used to treat interface roughness (18). If the film is ideally flat and uniform in thickness, multiple reflections from the upper and lower interfaces occur. In the general case, coherent as well as incoherent multiple reflections are possible and interference phenomena can be observed.

RESULTS

Oxidation of Bulk Fe-Cr-Ni -Y

Figures 2-4 show angle scans I(θ) for the 55Fe-25Cr-20Ni-0.3Y alloy. In these spectra, fluorescence signals from both the oxide layer and from the underlying bulk alloy contribute to I(θ). The most dramatic feature of these measurements is the systematic behavior of the Cr signal relative to that of Fe and Ni. Note that, with increasing oxidation, I(θ) for Cr grows, as shown in Fig. 2. However, the observed fluorescence intensities from Fe and Ni systematically fall with oxidation, even more rapidly than Cr increases. These systematics clearly show that a chromia scale is forming on the sample surface; the increasing Cr signal appears since the Cr concentration in Cr_2O_3 exceeds the Cr concentration of the substrate alloy. Fe and Ni, which appear at very low concentrations in the scale, become increasingly buried by the growing chromia overlayer.

If the oxide layer is thin, the signal in the high angle region (large θ) is predominately attributable to fluorescent radiation from the bulk substrate and, in the low angle region, predominately from the surface oxide. Because the oxide scales have larger indices of refraction than the substrate, they have lower critical angles. Consequently, the leading edge structure at low take-off angles will be enhanced with the appearance of the oxide scale. Consistently, the leading edge of the Cr signal (Fig. 2) shifts significantly to lower takeoff angle with increasing oxidation. The leading edge behavior for Fe and Ni emission are very different.

At the early stages of oxidation, the presence of transient iron oxide phases is apparent in the spectra. After the first displayed oxidation step (500° C), the Fe leading edge is shifted to lower emission angle (and Cr to higher angle). This indicates that iron oxides dominate the scale at this oxidation stage. However, by the second displayed oxidation step (600 C), the scale is strongly dominated by Cr_2O_3. Ni may not play a significant role in early stage scale formation.

Both Fe_2O_3 and Cr_2O_3 were also monitored using Raman spectroscopy (RS) in early stage oxidation of the Fe-Cr-Ni alloys (19). Although thermal histories and reactive element concentrations were different in the Raman and RXF experiments, it appears that the techniques provide complementary information. In the Raman experiments, samples were oxidized for one hour intervals at systematically increasing temperatures as the scale accumulated and samples were cycled to room temperature between oxidation steps. In those experiments, an Fe_2O_3 signal was first observed in Raman spectra after oxidation at 500-600 °C. Other signals, presumably from spinel-type structures (e.g.., FeO, Fe_3O_4, $FeCr_2O_4$, etc.) were observed at even lower temperatures. The Fe_2O_3 intensity grew as oxidation temperature was increased, then declined and eventually disappeared at 800 - 900 °C. A Cr_2O_3 signal first appeared between 700 - 800 °C and continued to grow in intensity as the scale thickened. Ni was not observed. The resolution of the present RXF system does not permit us to identify the different metal-oxide phases of a given element that might appear in the scale. For example, it is not possible to distinguish between FeO, Fe_3O_4 and Fe_2O_3 because the difference in critical angles for these compounds is less

than 2 mr. However, we can obtain an estimate of the elemental scale composition at early stages of oxidation.

It is clear from the RXF measurements that a predominately chromia scale forms on the alloy at the higher oxidation temperatures (T > 500 °C). However, the angular dependence of the Fe K_α radiation cannot be described solely by Fe radiation that originates in the underlying metal and is absorbed by the overlying chromia scale. These results point to the presence of Fe persisting in the scale, possibly in a dilute stratum just below the surface of the growing scale -- the transient Fe_2O_3 scale from an earlier stage in the thermal history may have converted into a spinel. The signal at the critical angle originates from emitters in a surface layer only 100-300 Å thick. The evolution of the intensity function $I(\theta)$ near the critical angle for Fe K_α radiation (Fig 3) shows that $I(\theta)$ initially decreases with increasing oxidation temperature, then eventually increases (3.5 hr @ 600 °C). The increasing signal after the 3.5 hr 600 °C oxidation means that the Fe concentration in the scale has begun to increase. Some increase in Ni concentration may also be apparent after this 600 °C oxidation (Fig 4). These results imply that, at 600 °C, Fe and Ni diffuse from the substrate into the scale (for this sample and thermal history). However, Figs. 3 and 4 show that Fe and Ni intensities, and hence concentrations in the scale, are very small at 600 C. Consequently, they do not significantly affect the absorption properties of the predominately chromia scale, thus justifying a relatively simple model for concentration estimation. . Fitting the 1 hr @ 600 °C experimental data with a suitable derivative of Eq [3] (17) gives the concentration of Fe in the scale that is ≈ 0.3-0.5% of the Fe concentration in the bulk (metallic alloy) sample. The same fitting procedure gives 1-1.2% after the 3.5 hr. oxidation at 600 °C . The concentration of Fe in the chromia scale appears to have gone through a minimum and was increasing at the termination of this series of measurements. Note that this procedure provides an estimate of the total Fe concentration in the scale but provides no information about the Fe oxidation state.

Film thickness

Because absorption lengths normally increase with increasing photon energy, the relative change in intensity for K_β lines traversing a sample of given thickness is smaller than the relative intensity change for K_α lines of the same element. Thus measured K_β/K_α intensity ratios obtained at a fixed high emission angle θ allow one to calculate the thickness of an overlying scale of known composition. We measure the K_β/K_α intensity ratio from the sample with an overlayer scale and normalize it to the K_β/K_α intensity ratio obtained from the scale-free substrate. Assuming a homogeneous substrate (which is considered to be unchanged by the developing scale), a homogeneous scale of thickness z_1 and making measurements at $\theta > 1.5*\theta_C$, a simple evaluation of scale thickness z_1 is possible. We obtain, at a given emission angle

$$\frac{K_\beta / K_\alpha(z_1)}{K_\beta / K_\alpha(z_1 = 0)} = \exp[\rho z_1(\mu_1 - \mu_2) / \sin\theta] \qquad [4]$$

where ρ is the density of the scale, μ_1 is the mass absorption coefficient of the scale at the wavelength of the K_α radiation and μ_2 is the mass absorption coefficient of the scale at the wavelength of the K_β radiation.

Using the measured Fe or Ni K_β/K_α ratios, chromia scale thicknesses are determined for the various stages of oxidation shown in Figs. 2-4. Recall that sequential oxidations were performed at systematically increasing temperatures; RXF measurements were done at the same elevated temperature, but in vacuum. After the one hour treatment at 600 C in 0.1 Torr of O_2, a scale $\approx$ 1 micron thick has appeared. After an additional 75 hr treatment in 10^{-7} Torr., the thickness has increased to $\approx$ 1.6 microns. The partial pressure of oxygen in a 10^{-7} Torr vacuum is high enough for oxidation to proceed (at an average oxidation rate of 66 Å/hr).

A series of measurements was done on another specimen of the same 55Fe-25Cr-20Ni-0.3Y alloy in order to closely track the growth of the chromia scale. Fig. 5 shows film thickness measurements obtained in-situ from K_β/K_α intensity ratios measured at a fixed angle as a function of oxidation time at 700 C in 0.1 Torr of oxygen. The scale thickness data provide measurements of oxidation rate in an isothermal environment. After 30 hours of isothermal oxidation, a scale $\approx$ 1 micron thick has developed. Assuming the parabolic law of oxidation is valid for this evolving scale, we obtain the oxidation constant 8.1×10^{-14} cm^2/sec. (The solid line in Fig. 5 is a parabolic fit to the data.) The corresponding mass gain parabolic rate constant, 2.2×10^{-12} $g^2cm^{-4}sec^{-1}$, is perhaps ten times larger than an extrapolation of the data compiled in ref. (20). A cross-section of the scale was also examined with SEM to confirm the scale thickness determined at the end point of the oxidation. The cross section shows that during isothermal oxidation at 700 C, an adherent scale was developed with a thickness of 1 - 1.2 microns (compared to $\approx$ 0.9 micron obtained from RXF). While this procedure (using the Fe or Ni K_β/K_α ratio) for measuring film thickness is insensitive to very thin films ($\approx$ 100 Å) as well as very thick films (several microns), it provides a convenient and reasonably accurate method for obtaining film thickness in the 0.02 - 1 micron range providing that the scale composition is known. For compositionally graded scales, more complex modeling procedures are needed to obtain thickness and depth profile information. For very thin films (tens to hundreds of Å) that are smooth and adherent to the bulk, interference phenomena in the fluorescence $I(\theta)$ that originates in the film or in the substrate can sometimes be exploited to determine the thickness. In the next Section, we present an example of such a case; oxidation of the β-NiAl intermetallic compound which forms an adherent aluminum oxide scale.

Oxidation of single crystal β-NiAl - interference phenomena

An angle scan of Al K_α radiation from a polished sample (10 Å rms roughness over $\approx$ 0.5 micron) of single crystal β-NiAl, taken prior to oxidation, is shown as solid dots in Fig. 6. The solid line is a fit to the experimental data using theoretical curves derived from equation [3]. It is clear that for the unoxidized bulk sample, our model is in good agreement with experiment. An angle scan taken after the sample had 5 hrs oxidation

exposure at 600 C is also shown in Fig. 6 (open circles). The shape of this curve can be explained by interference phenomena occurring in a thin film of Al oxide that has formed on the sample. Indeed, the relatively long wavelength (and coherence length) of the Al K_α radiation and the low electronic density of Al oxide make this system very favorable for the observation of an interference pattern.

The dashed line in Fig. 6 shows a fit of our model (using a derivative of Eq. [3]) to the experimental Al K_α data assuming a 170 Å thick Al oxide scale on the sample. This scale is similar in thickness to that measured in an x-ray grazing incidence reflectance (GIR) experiment (130 Å), from a sample oxidized in air at 600 °C for a comparable period of time, but experiencing a somewhat different thermal history (21).

Interference peak positions in $I(\theta)$ depend on the thickness of the scale and it's absorption properties. The interference maxima at 32 and 54 mr result from coherent multiple reflections of Al K_a radiation in the scale; this radiation primarily originates in the underlying bulk NiAl. The structure at 25 mr is attributable to fluorescing Al atoms located in the oxide film. As a first approximation in fitting the measured data, the parameters (density, absorption coefficients) of α-alumina were used. However, these parameters required adjustment in order to properly fit the data. The critical angle for the measured oxide film is about 1.5 mr smaller than that calculated for alumina. This suggests that the scale which developed during oxidation has a density about 12% lower than that of α-alumina.

It is well known that, at temperatures below ≈ 1000 °C, various transient forms of aluminum oxide will form in thermally grown alumina scales. Commonly, metastable cubic alumina scales such as γ,δ and θ. are formed (22-25). They all have different micro structures and form by different mechanisms. For example, θ-Al_2O_3 scales are less dense and grow more rapidly than α phase scales. Typically, transformation from a cubic transient phase to the hexagonal trigonal α phase results in ≈13% volume reduction. The cubic oxides generally form a defect structure, perhaps due to the relatively high rates of oxidation (22). Thus, it appears that the RXF measurements are sensitive to the reduced density of the transient alumina scale.

SUMMARY

Refracted X-ray fluorescence has been studied as a technique for investigating the evolution of thermally grown oxide scales. The measured fluorescence spectral function $I(\theta)$ has been analyzed for the geometric configuration in which measurements were made. Data were acquired, after varying degrees of oxidation, from specimens of Fe-25Cr-20Ni-0.3Y and from the intermetallic compound β-NiAl. Several techniques were developed to measure scale thickness. Transient phase behavior was clearly observed and monitored in evolving oxide scales.

It appears that RXF measurements can provide valuable information about the processes of oxidation which sequentially occur as a sample is oxidized. It has the potential to provide nondestructive depth profile information about scale composition to a depth defined by the penetration depth of the fluorescent x-rays. Depth scales that can be

effectively probed vary from angstoms (evanescent wave region) to microns (at large emission angles). Measurements acquired during isothermal oxidation allow for the extraction of scale growth rates, the evolution of transient phases, and, we expect, interface roughness. The technique can be developed for in-situ measurements and rapid data accumulation with the use of synchrotron radiation. Further modeling work is needed to quantify effects in I(θ) resulting from composition gradients and interface roughness effects.

ACKNOWLEDGEMENTS

Helpful conversations with K. Gray, K. Natesan, M. Grimsditch and D. Renusch are gratefully acknowledged.

REFERENCES

1. L. G. Parratt, Phys. Rev., **95**, 359 (1954).
2. B. L. Henke, Phys. Rev., **A6**, 94 (1972).
3. M Kamei, Y. Aoki et al., J. Appl. Phys., **74**, 436 (1993).
4. P. Eisenberger and W. C. Marra, Phys. Rev. Lett., **46**, 1081 (1981).
5. B. Lengeler, Adv. Mater., **2**, 123 (1990).
6. M. J. Bedzyk, G. M. Bommarito and J. S. Schildrrautt, Phys. Rev. Lett., **62**, 1376 (1989).
7. W. B. Yun, J. M. Bloch, J. Appl. Phys., **68**,1421 (1990).
8. R. S. Becker, J. A. Golovchenko and J. P. Patel, Phys. Rev. Lett., **50**, 153 (1983).
9. Y. C. Sasaki and K. Hirocawa, J. Appl. Phys.Lett., **58**, 1384,1991
10. T. Noma, A. Ida, K. Sakurai, Phys. Rev., **B48**,17525 (1993)
11. T. Noma, A. Ida, Rev. Sci. Instrum., **65**, 837 (1994)
12. P. deBokx, H. P. Urbach, Rev. Sci. Instrum., **66**,15 (1995)
13. T. A. Roberts, K. E. Gray, MRS Bulletin,**1**,43 (1995)
14. T. A. Roberts, D. H. Ko, K. E. Gray, Y. Y. Wang, R. P. Chang, S. Ogawa, Appl. Phys. Lett., **66**, 2054 (1995)
15. R. W. James, The Optical Principles of the Diffraction of X-Rays, Cornell Univ. Press, Ithaca, (1965)
16. H. P. Urbach, P. K. de Bokx, Phys. Rev., **B53**, 3752 (1996).
17. I. Koshelev, A. P. Paulikas, and B.W. Veal, to be published
18. P. Beckmann, A Spizzichino, The Scattering of Electromagnetic Waves from Rough Surfaces, Artech House Inc., Norwood (1987)
19. D. Renusch, B. Veal, K. Nateson, M. Grimsditch, Oxidation in Metals, to be published.

20. H. Hindam and D. P. Whittle, Oxidation of Metals, **18**, 245, 1982
21. G. Muralidharan, X. Z. Wu, Hoydoo You, A. P. Paulikas and B. W. Veal, Proceedings of this symposium
22. J. Doychak, J. L. Smialek, T. E. Mitchell, Met. Trans., **A20**, 499 (1989).
23. M. W. Brumm, H. J. Grabke, Corrosion. Sci., **33**, 1677 (1992).
24. B. A. Pint, J. R. Martin, L. W. Hobbs, Sol.St.Ionics, **78**, 99 (1995).
25. C. Rybiki, J. Smialek, Oxidation in Metals, **31**, 275 (1989).

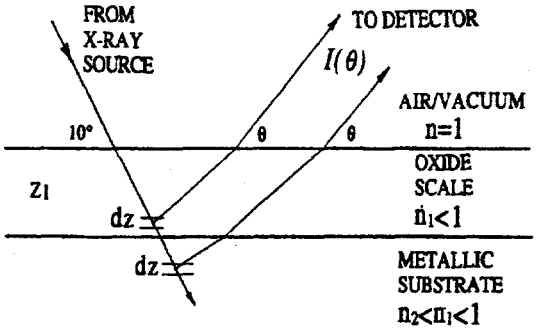

1. Schematic illustration of refracted x-ray fluorescence (RXF) experiment.

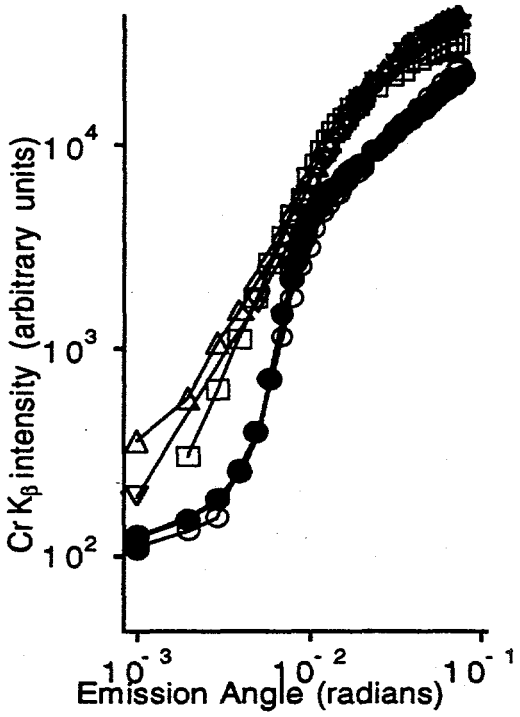

2. Cr Kβ fluorescence intensities from the 55Fe-25Ni-20Cr-0.3Y alloy after different levels of oxidation. Legend for figures 2, 3, and 4: full circles-30°C in vacuum, unoxidized; open circles-after 1 hr at 500°C in 0.1 Torr O_2; squares-after 1 hr at 600°C in 0.1 Torr O_2 and 15hr in 10^{-7} Torr vac; pyramids-after a total of 90hr in 10^{-7} Torr vac; inverted pyramids-after an additional 3.5 hr at 600°C in 0.1 Torr O_2 and 9 hr in 10^{-7} Torr vac

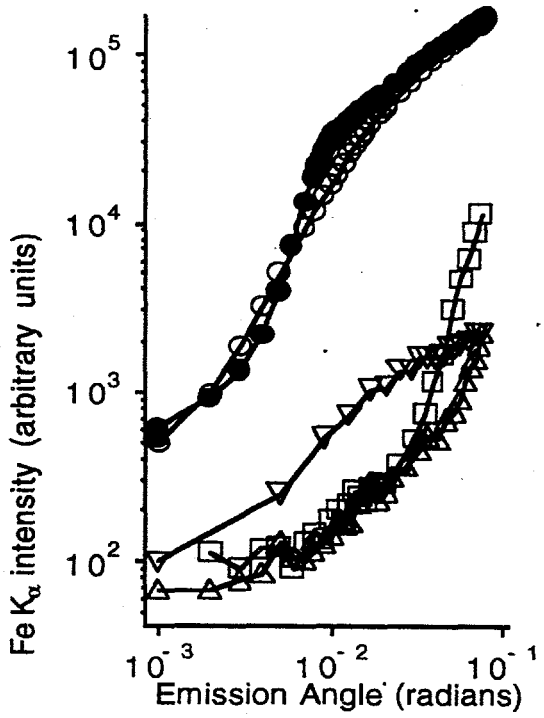

3. Fe K_α fluorescence intensities from the 55Fe-25Ni-20Cr-0.3Y alloy after different levels of oxidation.

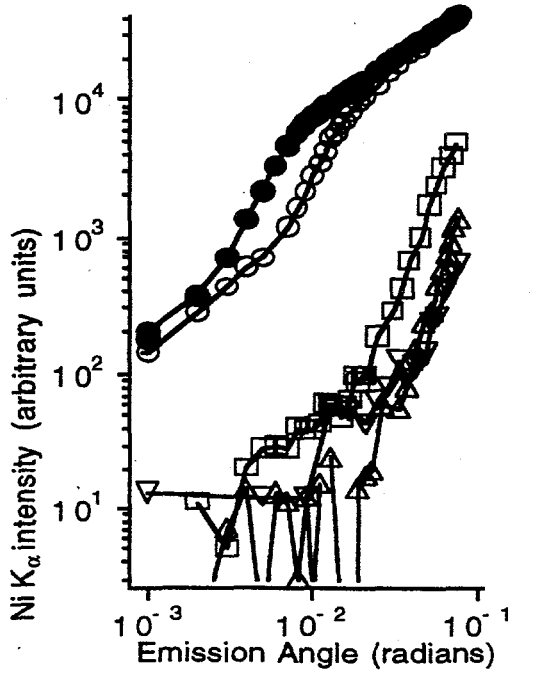

4. Ni K_α fluorescence intensities from the 55Fe-25Ni-20Cr-0.3Y alloy after different levels of oxidation.

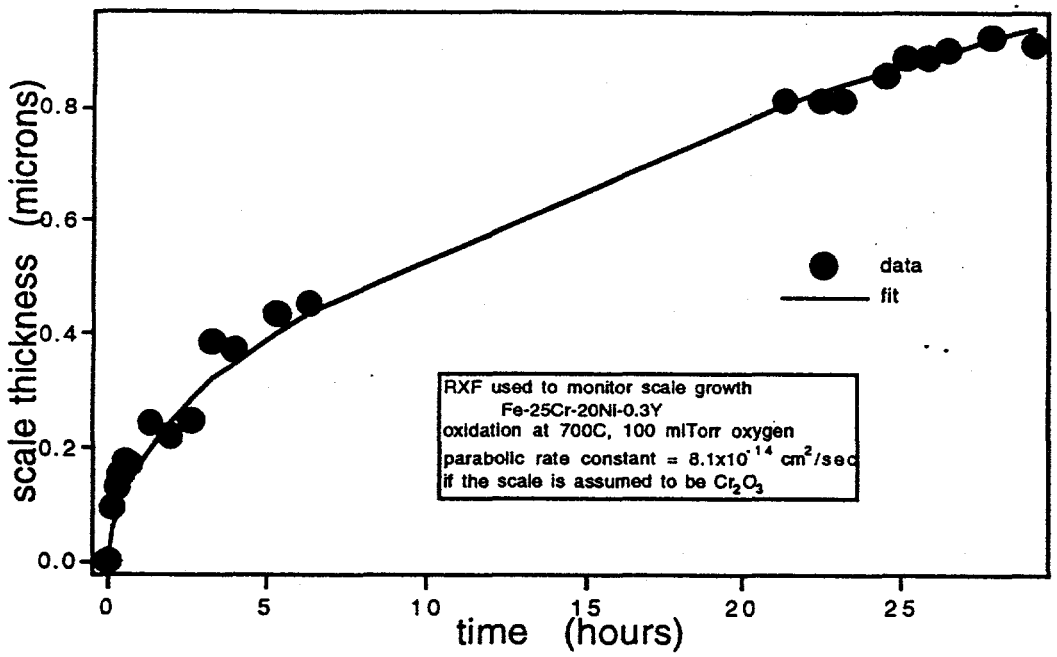

5. Measured thickness, using RXF, of the accumulating oxide scale thermally grown at 700 C in 0.1 Torr. O_2 on the 55Fe-25Ni-20Cr-0.3Y alloy.

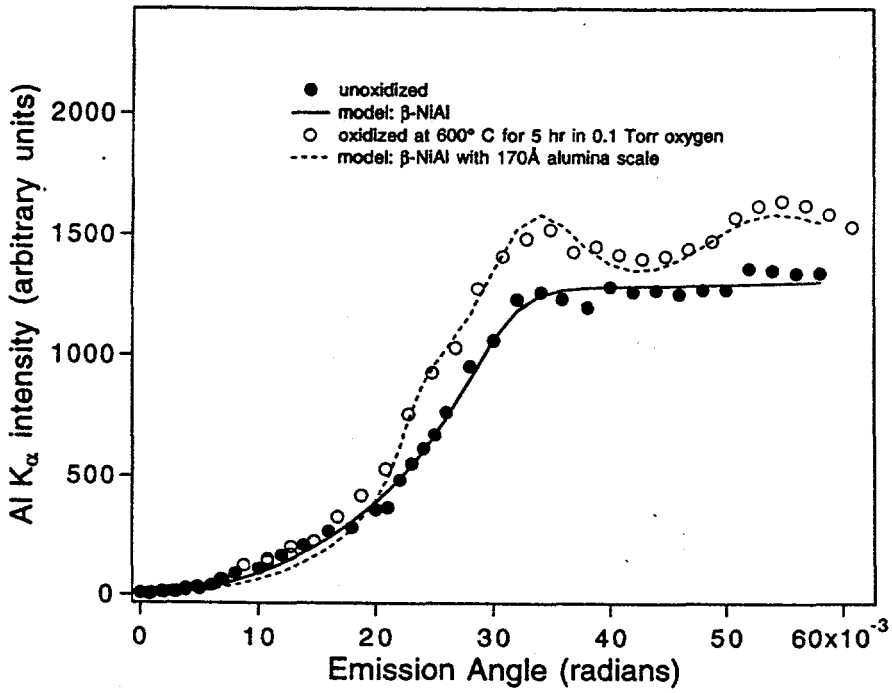

6. Al K_α fluorescence intensities from β-NiAl before and after oxidation at 600 C. The Al K_α signal for the oxidized sample shows interference phenomena. Solid and dashed lines are model calculations.

Key Words

x-ray fluorescence
oxidation
chromia scale
alumina scale